

ACCEPTED VERSION

Manabendra Saha, Giovanni Gitto, Bassam B. Dally

Burning characteristics of grape marc under mild combustion conditions

Experimental Thermal and Fluid Science, 2020; 114:110059-1-110059-11

© 2020 Elsevier Inc. All rights reserved.

This manuscript version is made available under the CC-BY-NC-ND 4.0 license

<http://creativecommons.org/licenses/by-nc-nd/4.0/>

Final publication at: <http://dx.doi.org/10.1016/j.expthermflusci.2020.110059>

PERMISSIONS

<https://www.elsevier.com/about/policies/sharing>

Accepted Manuscript

Authors can share their [accepted manuscript](#):

24 Month Embargo

After the embargo period

- via non-commercial hosting platforms such as their institutional repository
- via commercial sites with which Elsevier has an agreement

In all cases [accepted manuscripts](#) should:

- link to the formal publication via its DOI
- bear a CC-BY-NC-ND license – this is easy to do
- if aggregated with other manuscripts, for example in a repository or other site, be shared in alignment with our [hosting policy](#)
- not be added to or enhanced in any way to appear more like, or to substitute for, the published journal article

9 June 2022

<http://hdl.handle.net/2440/123603>

Journal Pre-proofs

Burning characteristics of grape marc under mild combustion conditions

Manabendra Saha, Giovanni Gitto, Bassam B. Dally

PII: S0894-1777(19)31799-6

DOI: <https://doi.org/10.1016/j.expthermflusci.2020.110059>

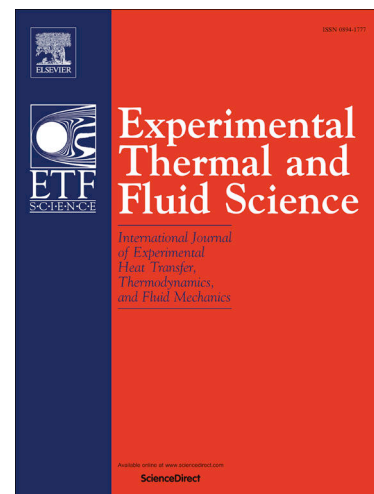
Reference: ETF 110059

To appear in: *Experimental Thermal and Fluid Science*

Received Date: 26 October 2019

Revised Date: 24 December 2019

Accepted Date: 23 January 2020



Please cite this article as: M. Saha, G. Gitto, B.B. Dally, Burning characteristics of grape marc under mild combustion conditions, *Experimental Thermal and Fluid Science* (2020), doi: <https://doi.org/10.1016/j.expthermflusci.2020.110059>

This is a PDF file of an article that has undergone enhancements after acceptance, such as the addition of a cover page and metadata, and formatting for readability, but it is not yet the definitive version of record. This version will undergo additional copyediting, typesetting and review before it is published in its final form, but we are providing this version to give early visibility of the article. Please note that, during the production process, errors may be discovered which could affect the content, and all legal disclaimers that apply to the journal pertain.

© 2020 Elsevier Inc. All rights reserved.

BURNING CHARACTERISTICS OF GRAPE MARC UNDER MILD COMBUSTION CONDITIONS

Manabendra Saha^{*}, Giovanni Gitto and Bassam B. Dally

Centre for Energy Technology, School of Mechanical Engineering,
The University of Adelaide, SA 5005, Australia

*e-mail of corresponding author: manabendra.saha@adelaide.edu.au

Abstract

In this experimental study, the burning characteristics of grape marc, as a biomass fuel, under MILD (Moderate or Intense Low-oxygen Dilution) combustion conditions are explored. Specifically, the impact of grape marc particle size on flame structure, stability and pollutant emissions, under MILD combustion, is investigated. Three different particle sizes of the grape marc are considered, in the range of 150 - 250 μm , 250 - 355 μm and 355 - 500 μm . The particles are injected through a central insulated jet into a hot and vitiated coflow inside a vertical MILD combustion furnace. All other operating conditions remain the same. CO_2 is employed as a carrier gas and the central jet bulk Reynolds number is set to the value of $\text{Re}_{\text{jet}} = 13,040$. The vitiated coflow had $\sim 6\%$ oxygen molar fraction and a flow bulk temperature of about $T_{\text{co-flow}} = 1330\text{K}$. The heat input from the grape marc fuel is kept constant at 10 kW, corresponding to a mass flow rate of 1.63 kg/hr. Stable MILD combustion conditions have been successfully achieved for all cases. The temperature gradient along the vertical and the radial direction of the furnace is limited to below 100 K for all the cases. The variation of particle size does not significantly impact on the furnace temperature and exhaust emissions. Albeit, the case of largest particle size exhibits a higher temperature by $\sim 40\text{K}$ as compared to the other two cases, and the highest NO production is identified for the middle particle size's case showing peak value of approximately 478 ppm at the exhaust at 3% excess O_2 . No remarkable NO-reburning process is observed for any cases, which points towards the intense volatile combustion of grape marc under MILD combustion conditions.

Keywords: Grape marc, MILD combustion, Particle size, Temperature, CO_2 , NO.

Introduction

Biomass is considered to have a crucial role as a replacement of traditional fossil fuels, especially those that come from agriculture waste [1]. Versatile advantages distinguish biomass from other renewable fuel sources [2]. Biomass can be a carbon-neutral energy source and can even act as a Green House Gases (GHGs) negative emitter. The quantity of carbon-dioxide absorbed by biomass throughout its lifecycle, via the photosynthesis process, can significantly compensate for its emissions during combustion [3]. Bioenergy accounts for a large portion of the global energy which has a theoretical potential to produce about 3500 EJ/year [4]. Bioenergy currently supplies approximately 9% of the global energy consumption and according to REN21 report, it is expected to grow significantly, to reach 12.4% in 2023 [5] and to be the predominant source of renewable energy. The current work is concentrating on the implementation of eco-friendly and environmentally-safe technologies for biomass utilisation as an energy resource.

The present research concentrates on the utilisation of the grape marc as a biomass fuel for energy production. Grape marc is made of grape skins, seeds, pulp and stalks; while it is a solid waste residue throughout the wine-making process from grape pressing [6]. It has been estimated to account for approximately 22% of the annual crush in small-sized wineries and this percentage can drop down to about 11% in larger-scale ones. [7]. The Food and Agriculture Organization of the United Nations estimates that the residue from the wine industry worldwide exceeds 20 million tonnes annually. While in Australia, the grape crush was quantified to be approximately 1930,000 tonnes in 2017 and 863,788 tonnes of those were coming from South Australia [8]. According to the Muhlack et al. [9], grape marc accounts for 10–30% of the mass

of grapes crushed during the winemaking process, resulting in several hundred thousand tonnes of grape marc in Australia alone. Currently, this large waste volume is simply disposed of, and then dumped or settled in ponds by the majority of the wineries and it constitutes a non-negligible operating cost [7]. Hence, there is a substantial unexploited potential for renewable energy generation using the residues of the wine industry. As a fuel, grape marc has a significantly higher volatile matter content (of approximately 69% db) and less fixed carbon (about 26% db) comparing to Victorian brown coal [6]. However, a high moisture content (of about 65%) of both fuels [6] diminishes the overall efficiency of the combustion process. There are two main conventional methods to combust biomass, namely; fluidised-bed and grate combustors [9].

One of the major issues associated with grape marc combustion is the high nitrogen content and the resulting NO_x emission. Miranda et al. [10] investigated the combustion of grape marc mixed with Pyrenean oak using thermogravimetry and found that a significant increase of NO emissions during dilution of grape marc with Pyrenean oak. Combustion characteristics of grape marc and sawdust (50%-50%) mixture were also investigated in a 12 kW boiler [11] and the measured exhaust NO is found to be 456 mg/Nm^3 at 10% excess O_2 , which is equivalent to 560 ppm at 3% excess O_2 . Therefore, there is an urging need to utilise novel technologies to overcome this problem while ensuring efficient and eco-friendly combustion of grape marc. Typically, particulate matter (PM) is a complex mixture of extremely small particles of mineral matter that is generated from the combustion of hydrocarbon fuels [12]. The formation and composition of PM vary significantly with fuel types and combustion conditions, such as surrounding local oxygen concentrations and local temperature of the combustion chamber/furnace [13]. Nonetheless, the PM is predominantly affected by the combustion temperature that causes physical, chemical, and morphological changes for the biomass

combustion and gasification [14]. As the temperature is increased, particulate diameter decreases, following a shrinking core phenomenon, altering the chemical properties of particulates and increase residual solid carbon and inorganic content [14]. The PM emissions were reported in the range of 20 to 40 mg/Nm³ at 10% O₂ concentration for the conventional combustion of grape marc in a domestic boiler of 40 kW capacity [15]. Kariem et al. [11] reported the combustion tests of grape marc-saw dust (50-50 wt%) pellet of 26 mm length in a 12-kW capacity industrial boiler where the PM was found to be 703 mg/Nm³ at 10% O₂ concentration. The formation of a high concentration of PM was mainly due to the high ash content of wood residues/ sawdust [11]. The relationship between NO formation and PM emissions is not well-established [16]. Yu et al. [16] investigated the impacts of low-NO_x combustion technologies on PM emissions from coal-fired boilers. They reported that low-NO_x combustion (i.e., air staged combustion) results in lower concentrations of PM 2.5 (particulate matter of 2.5-micron diameter or less) and PM1 (particulate matter of 1-micron diameter or less) owing to the activation of solid-vapour-particle processes [16]. McElroy et al. [17] reported that the boilers with high NO emissions had higher flame temperatures, which enhanced ash vaporization and led to high PM emissions.

A feasible solution to assure high burning efficiency while maintaining the NO_x formation at sustainable levels is the direct recirculation of the combustion products (exhaust gas) inside the combustion chamber [18]. This combustion technology is called Moderate or Intense Low-oxygen Diluted (MILD) combustion or “volumetric combustion” which produces a semi-uniform thermal field inside the combustion chamber, improves combustion efficiency and emits low amounts of NO_x [19]. Owing to these unique features of MILD combustion, it is speculated that PM emission suppressed under these conditions. Weber et al. [20] reported the

PM emission for heavy fuel oil combustion under MILD condition is found to be 20 mg/Nm^3 using a new atomizer. A series of experimental and numerical studies have been conducted on the MILD combustion characteristics of conventional fossil fuel such as pulverised coal so far [21-32]. While the MILD combustion of biomass fuels is still in an infancy stage. Very limited studies have been conducted for the application of MILD combustion to biomass fuels [33-37]. Wang et al. [38] reported a numerical study of biomass combustion under Oxy-MILD mode and hinted that biomass MILD combustion has a great potential to attain “negative CO_2 emissions”. Nonetheless, no study has been found which reports the burning characteristics of grape marc and the impact of fuel particle size on the combustion stability and pollutant emissions under MILD combustion mode.

The present work aims to deepen our understanding of the burning characteristics of grape marc as a biomass fuel under MILD combustion conditions. It reports the outcome of an experimental investigation of pulverised grape marc with different particle sizes in the range $150 - 250 \text{ }\mu\text{m}$, $250 - 355 \text{ }\mu\text{m}$ and $355 - 500 \text{ }\mu\text{m}$. In-furnace temperature distribution, in-furnace gas concentrations and exhaust emissions of O_2 , CO_2 , CO and NO_x are reported and discussed.

Experimental Setup and Operating Conditions

The experimental campaign was conducted on a vertical MILD combustion furnace as shown in Figure 1. The furnace has a height of 1200 mm and a cross-section area of $260\text{mm} \times 260\text{mm}$. The detail description of the experimental setup has been provided previously [25], whilst a very brief description of the experimental method is provided here below. The furnace is supplied with a hot and vitiated coflow supplied by a secondary burner which stabilises a turbulent non-premixed swirl flame of natural gas. The secondary swirl burner also controls

the main furnace's wall temperature. When steady-state conditions are achieved, and the in-furnace temperature is stabilized above a threshold value of approximately $\sim 1200\text{K}$, the grape marc was injected into the furnace using CO_2 as a carrier gas through the central insulated fuel jet. Fuel particles emerge from the jet into the hot coflow and auto-ignition occurs inside the furnace. The experimental conditions are summarised in Table 1.

The temperatures were measured simultaneously using R-Type thermocouples. A steady-state energy balance equation is used on the thermocouples' bead surface for radiation temperature corrections following a procedure developed in previous work [25]. The calculations show that the maximum radiation correction is less than 2.5% of thermocouples' measurement. The exhaust and in-furnace gas concentrations are measured using TESTO Model 350XL gas analyser. The measurements errors were ± 10 ppmv for CO , ± 5 ppmv for NO , and $\pm 0.8\%$ for O_2 of the measured value.

Table 1. Experimental conditions for the stable MILD combustion of grape marc.

Experimental Cases	Case 1	Case 2	Case 3
Particle sizes (μm)	150 - 250	250 - 355	355 - 500
Jet Reynolds number, Re_{jet}	13,040	13,040	13,040
Global equivalence ratio, ϕ	0.85 ± 0.01	0.90 ± 0.02	0.92 ± 0.01
Furnace wall temperature (K)	1130 - 1210	1140 - 1220	1140 - 1215
Heat input by grape marc (kW)	~ 10.0	~ 10.0	~ 10.0
Particle residence time (ms)	208	208	208
Co-flow O_2 (v/v % db)	6	6	6

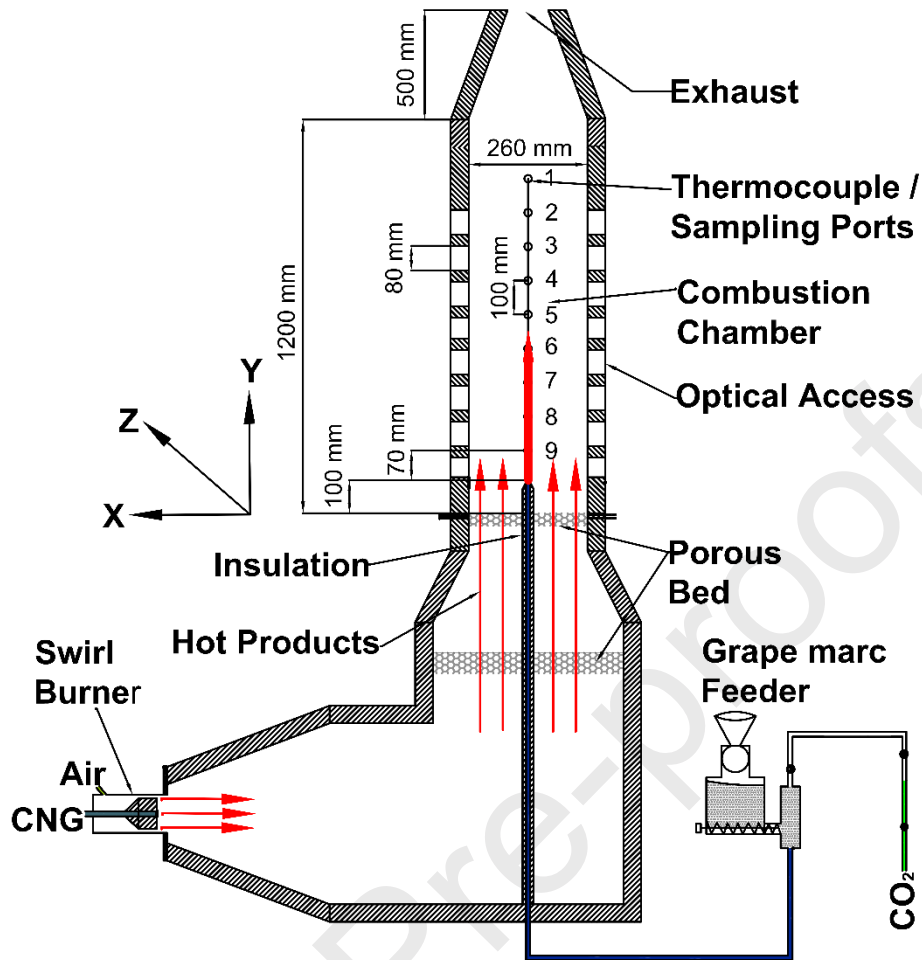


Figure 1. Sketch of the MILD Combustion Furnace Setup

Characteristics of grape marc

In April 2015, the grape marc was collected from the Riverland region of South Australia. The grape marc was dried in an electric oven for 6 hours at 105°C. The gross dry calorific value of grape marc is measured to be 22.2 MJ/kg. The grape marc is milled and sieved into three different size ranges as detailed in Table 1. The ultimate and proximate analysis of the grape marc is reported in Table 2. The absolute errors of the carrier gas flow-rate measurements were $\pm 2\%$, and the grape marc mass flow-rate was found to be $\pm 2.5\%$.

Table 2. Grape marc analysis.

Ultimate analysis (wt% dry ash free)					Proximate analysis (wt %, db)		
C	H	O _{by difference}	N	S	Fixed carbon	Volatile matter	Ash
51.49	6.52	37.71	2.74	1.54	24.98	65.66	9.36

Results and Discussion

To investigate the effect of the fuel particles' size on the burning characteristics of grape marc under MILD combustion conditions three different cases have been analysed. Each case had the same exact operating conditions but different particles' size: 150 μm – 250 μm range, 250 μm – 355 μm range and 355 μm – 500 μm range. CO_2 is employed as a carrier gas and the central jet bulk Reynolds number is set to the value of $\text{Re}_{\text{jet}} = 13,040$. The coflow was introduced into the furnace by a secondary swirl burner generating a hot vitiated co-flow with ~6% excess oxygen on a molar basis and a flow bulk temperature of about $T_{\text{co-flow}} = 1330$ K. The heat input from the grape marc fuel is kept constant at 10.0 kW, corresponding to a mass flow rate of 1.63 kg/hr.

In-furnace Visual Observation

The visual appearance of the inside of the furnace, for the three experimental cases, is shown in Figure 2. The images were taken through three windows located on the side of the vertical furnace: A) bottom ($y = 80$ mm), B) middle ($y = 500$ mm) and C) top ($y = 995$ mm).

No visible flame has been observed for any of the analysed experimental configurations. In each case, the thermal field, determined from the wall colours, appears to be uniformly distributed. However, it is clear that a higher luminosity is noticeable inside the furnace with the increase of the particles' size. Switching from the 150 μm – 250 μm particles' size case to the 355 μm – 500 μm , the walls seem to turn from a light red colour to a brighter yellowish one.

Despite the absence of a conventional clearly detectable visible flame, it is possible to notice the presence of glowing particles coming upwards along with the furnace with the gas stream, which increases in intensity with the fuel particles' size. These glowing particles appear to be concentrated mainly in the middle region of the furnace for all the cases.

The bottom part of the furnace is largely dominated by the volatiles' release and their reaction, following the fast pyrolysis of the particles through radiation from the hot walls and interaction with hot coflow. Moving up to the middle region, glowing particles are visible since they have been heated to a temperature where char burnout would have started, resulting in the glowing appearance. Further downstream, in the top part of the combustion chamber, only some glowing particles are still visible because the solid char combustion is ending and ashes and unburned carbon is moving upward toward the exhaust duct. Glowing particles are less visible in the 150 μm – 250 μm case because of the large surface to volume ratio that makes the heating process faster, the smaller bright emitting area and the earlier devolatilisation process.

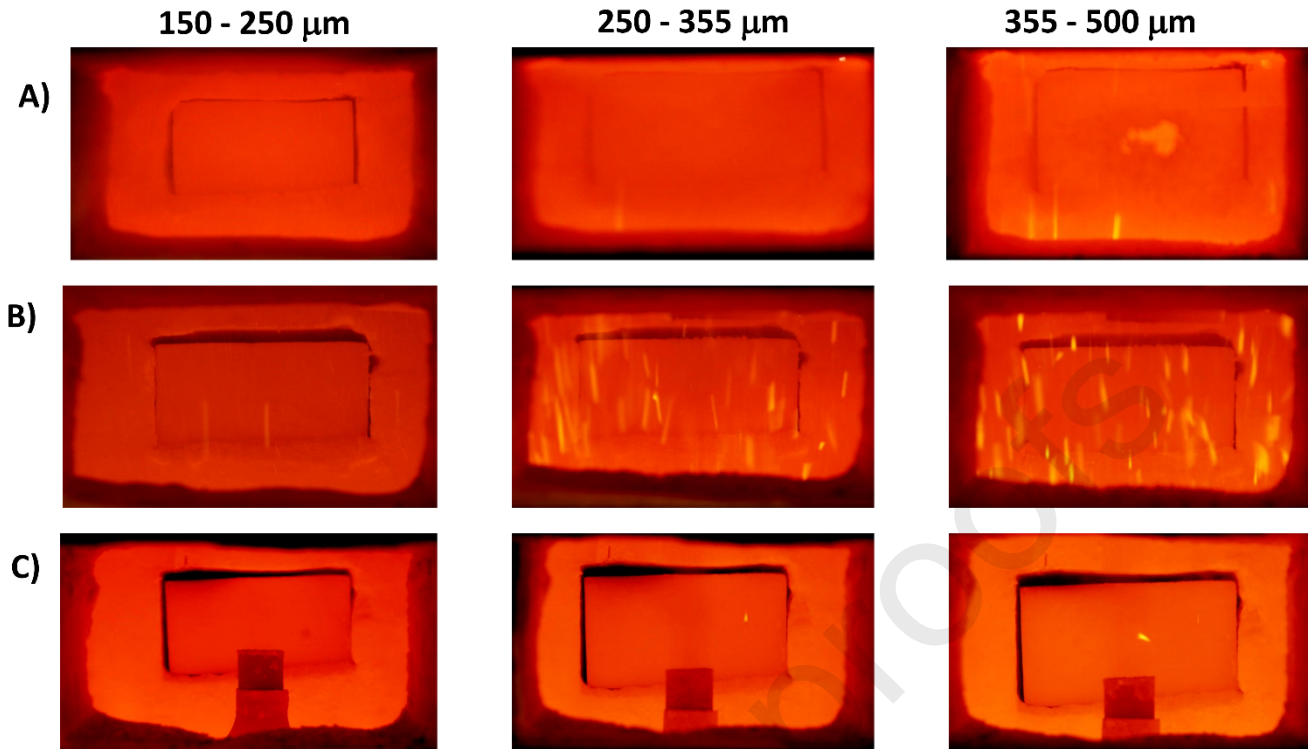


Figure 2. In-furnace visual observation

In-furnace Temperature Distribution

In Figure 3, the measured mean temperature contour plots for the three investigated cases are presented. The reported temperature values have been measured along the furnace's middle section ($x = 0$ mm) at different vertical locations spaced 100 mm apart, starting at 70 mm ($y = 170$ mm) and up to 770 mm ($y = 870$ mm) above the central jet exit. A similar scan horizontally, 100 mm from the centreline, has also been considered. A semi-uniform thermal field inside the combustion chamber can be observed for all the analysed cases. This means that MILD combustion conditions have been successfully achieved. The temperature gradient along the vertical and the radial direction is limited to below 100 K for all the cases. The comparison between the three cases points to a small increase in the temperature level with bigger particles' diameter. This trend is consistent with the brighter appearance observed for the largest particle sizes. A relatively cold region showing the minimum temperatures inside

the furnace is identified above the CO₂ central jet exit for all the cases. This is due to the low temperature of the carrier gas stream inside the central jet that needs to be heated up once entered the furnace. However, such a region appears to be located closer to the central jet exit for the 150 μm – 250 μm case when compared to the 250 μm – 355 μm and 355 μm – 500 μm cases.

It is clear that the location of major heat release, translated into a peak in the measured centreline temperature differs from one case to another. Also clear is that the case with the largest particle size exhibit a higher temperature by $\sim 40\text{K}$ as compared to the other two cases. Noteworthy is the fuel flow rate, and the flow rate of CO₂ (as carrier gas) and the co-flow conditions are the same for the three cases. The slight increase in the temperature level at the bottom of the furnace where the co-flow and central jet temperatures have a predominant influence can be explained with an enhanced heat flux coming down with the recirculation of the gases. A possible interpretation for the faster heating up of the region above the central jet exit for smaller particle sizes could be the earlier volatiles release and combustion. As it has been found for the coal [31], an increase in the particle sizes leads to a delayed and further downstream devolatilisation process. Moreover, the higher surface to volume ratio of the small particles allows the heat transfer to be faster, contributing to the earlier volatile release and the subsequent temperature rise.

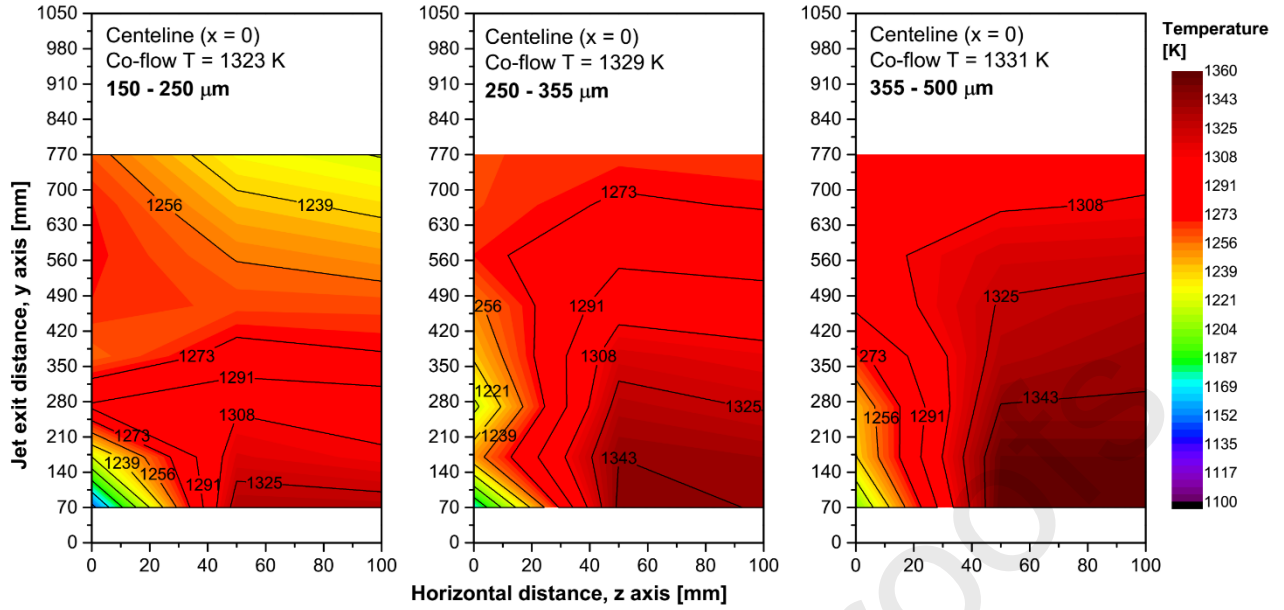


Figure 3. Mean temperature distribution for one half in the middle of the furnace

Figure 4 shows the measured, in-furnace, average temperature profile along the vertical direction (y axis) at three different radial positions, namely $z = 0$ mm (centreline), $z = 50$ mm and $z = 100$ mm. All measurements are performed along the same furnace side ($x = 0$ mm plane) and for the three investigated cases are shown together for comparison purposes.

The temperature profiles show a variation along the vertical axis smaller than 100 K for all the radial distances and all the particle sizes, consistently with what has been highlighted before. The graphs for $z = 50$ mm and $z = 100$ mm clearly highlight a decreasing trend of the temperature along the vertical axis. Moreover, it is easy to notice a slightly higher overall temperature level with the increasing of the particles' size. However, the temperature profile along the centreline shows a different trend. For all the analysed cases, an initial temperature rise due to the heating up of the relatively cold CO_2 jet is identified, and it is followed by a plateau over the second half of the furnace. Even though higher temperature values are shown for larger particles at the jet exit and at the top of the furnace, a different behaviour among the three cases is shown along the y axis. The case with small size particles, 150 μm – 250 μm , exhibit a steep increase in temperature with a peak appearing at 270 mm. While for the case

with the medium and large particles' size, a smaller peak appears at 170 mm followed by a gradual increase for a higher position within the furnace.

This small difference in centreline temperature is perhaps attributed to the rate of carbon burnout and delayed heat release is influenced by the particles' size. At locations away from the centreline, a slight decrease in the measured temperature and a constant temperature difference between each of the cases.

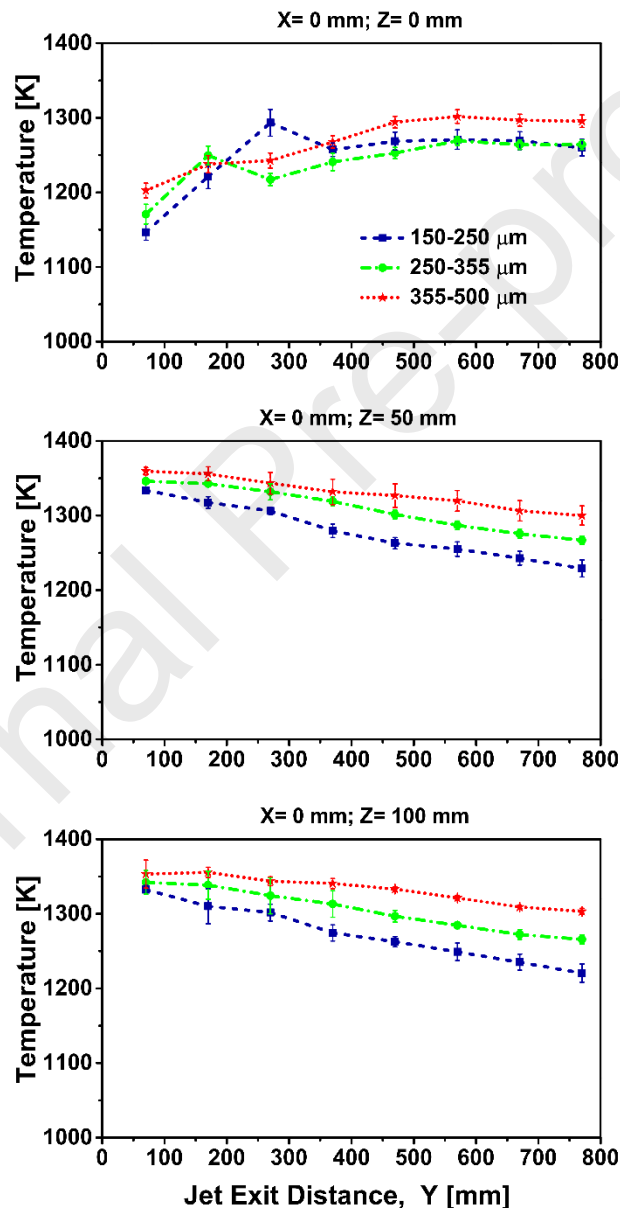


Figure 4. In-furnace temperature profiles

In-furnace Species Concentration

Measurements of the gas composition inside the furnace are presented in Figures 5-10, and they include the mean mole fractions of CO_2 , CO , O_2 , and NO at different locations inside the furnace. The sampling locations are the same ones considered for the thermal field study. All the measurements are performed along the furnace central plane ($x = 0$ mm), at 9 different vertical positions (from $y = 170$ mm to $y = 970$ mm) and for three radial locations ($z = 0$ mm, $z = 50$ mm, $z = 100$ mm).

Mean CO_2 molar fraction profiles along the y axis for the three cases are reported in Figure 5. It is possible to notice similar CO_2 content among the cases at the bottom and top of the furnace. The $z = 0$ mm profiles show a decreasing trend along the vertical direction for all the particle sizes. A similar continuous decrease is identified for the $250\text{ }\mu\text{m} - 355\text{ }\mu\text{m}$ and $355\text{ }\mu\text{m} - 500\text{ }\mu\text{m}$ cases. However, the $150\text{ }\mu\text{m} - 250\text{ }\mu\text{m}$ case shows an earlier and steeper reduction followed by a slight rise approximately at the middle of the vertical height. At $z = 50$ mm location, all the cases have been found to follow the same trend. The CO_2 molar fraction is observed to be increasing along the vertical direction. However, the measured values level slightly increases for bigger particles sizes. Very small discrepancies are observed between the behaviours of the analysed cases at $z = 100$ mm. Being far from the central jet where the fuel injection and the reaction occur, the influence of the co-flow CO_2 molar fraction is predominant. For all the particles sizes, low values are measured with a small increase at a higher location on the y axis. For the large particle case, only a peak is observed 570 mm from the jet exit.

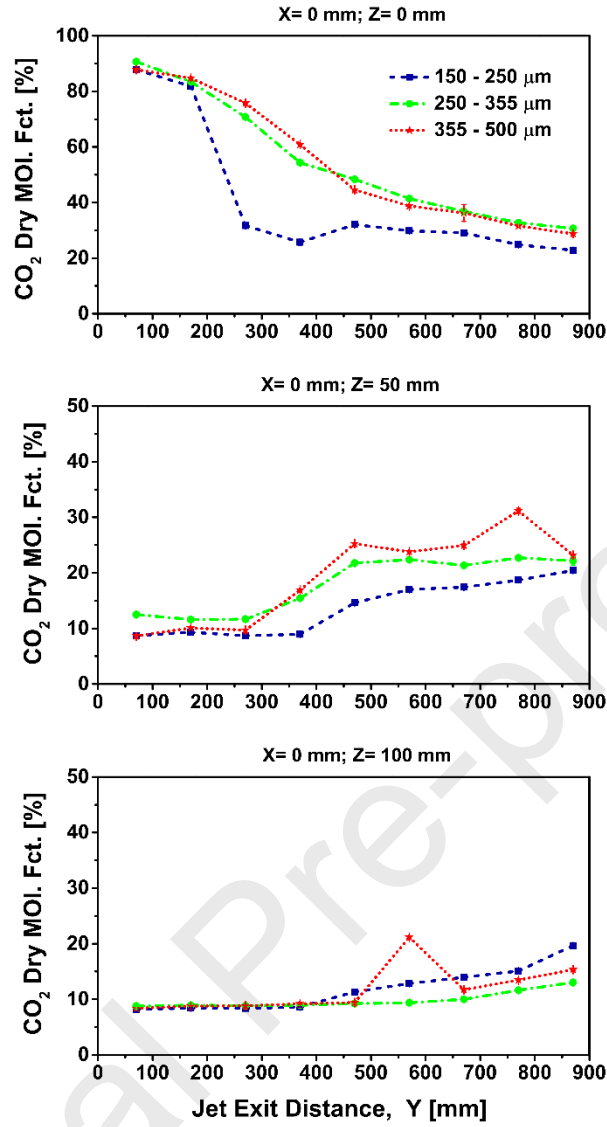


Figure 5. In-furnace CO₂ molar fraction

Figure 6 shows the mean CO₂ molar fraction distribution for a central plane of the furnace and for the three cases. Comparing the three contours, a general trend can be identified for all cases. The highest values of mean CO₂ molar fraction are measured in the region above the central jet exit, as expected since pure CO₂ is employed as a carrier gas. The lowest CO₂ concentrations are located at the bottom of the furnace for high radial distances from the centreline ($50 \text{ mm} < z < 100 \text{ mm}$) with values similar to the one measured in the co-flow. Hence, a significant CO₂ molar fraction gradient is measured along the radial direction at the bottom of the furnace. For

higher positions, a decreasing trend is clearly noticeable along the centreline while an increase in the CO₂ content is identified for higher radial distances. Such trends continue till the top where the radial gradient is consistently reduced even though still noticeable. The centreline decay of the CO₂ mean mole fraction decreases rapidly for the low particle size case while it extends further downstream for larger particle sizes. For the 150 µm – 250 µm case only it is possible to notice a small rise in the CO₂ molar fraction along the centreline after the rapid decrease above the jet exit. The flow field inside the furnace is equal for all the cases since the Reynolds' number is kept constant ($Re_{jet} = 13040$). Hence, the different CO₂ distribution among the central jet exit may be due to a difference in the volatile release and their reaction with the coflow. The release of volatile matters makes the CO₂ molar fraction decreasing due to the mixing with the combustion products. Moreover, the heterogeneous char combustion reaction ($C_{char} + CO_2 \rightarrow 2CO$) occurring after the devolatilisation process consumes CO₂ further decreasing the molar fraction [26, 39]. Therefore, it probably means that the location of the volatile's releases and the start of the reaction is switched further downstream with the increasing of the particles size. The small increase in the CO₂ content identified for the 150 µm – 250 µm case along the centreline could be associated with a CO₂ production during the oxidation reaction of the CO produced in the volatiles and char combustion. This increase also coincides with an increase in the temperature, as seen in Fig. 4 at the same location.

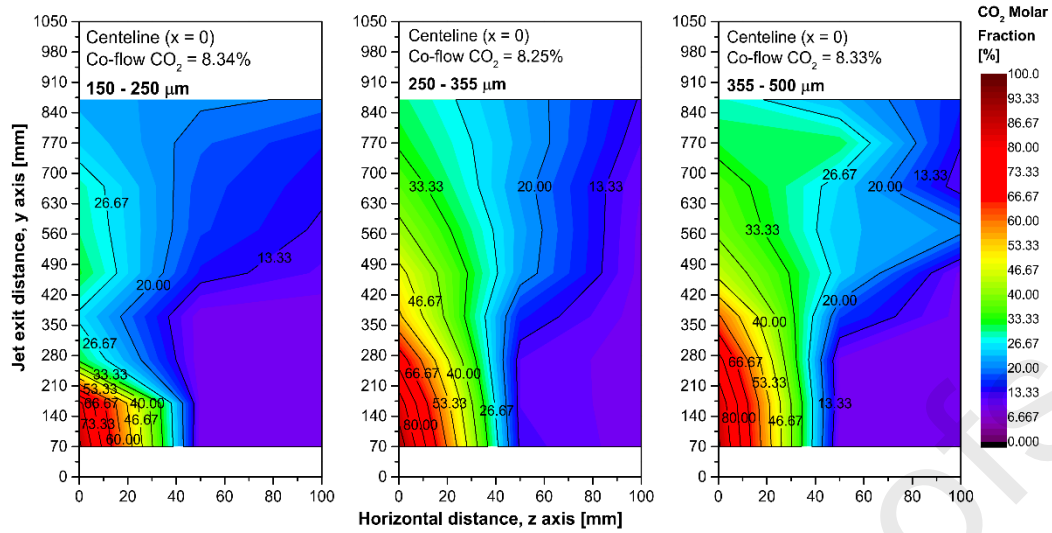


Figure 6. In-furnace CO₂ molar fraction distribution for one half in the middle of the furnace

Figure 7 presents the CO molar fraction vertical variation. Higher values of CO concentration are observed for smaller particles sizes for each of the three radial positions investigated. However, such a discrepancy tends to become less evident moving from $z = 0$ mm to $z = 100$ mm. Globally, the mean CO molar fraction values measured along the centreline are higher than the ones at further radial distances. Furthermore, the CO vertical profiles for the 250 μm – 355 μm and 355 μm – 500 μm cases at 50 mm and 100 mm away from the centreline show a smooth and continuous increasing trend. The 150 μm – 250 μm case instead has a discontinuous trend, in particular along the centreline where it is observed to have a peak at approximatively the middle height of the furnace.

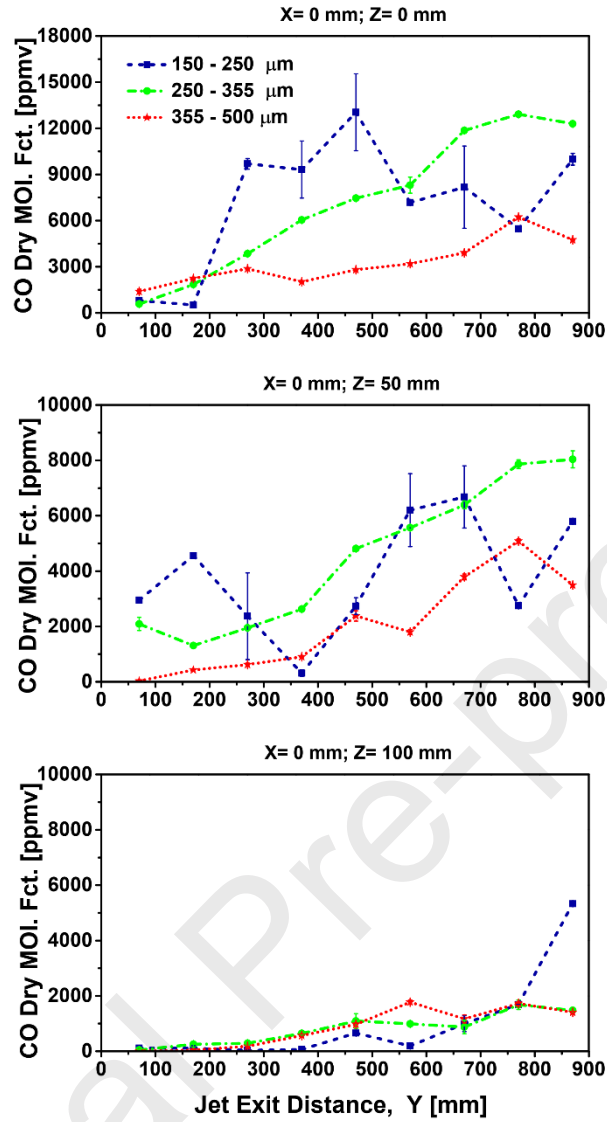


Figure 7. In-furnace CO molar fraction

In Figure 8, the mean CO molar fraction distribution is shown. The comparison of the three contour plots for the analysed cases clearly highlights a global CO molar fraction reduction with the increase of the particle size. Peak values of the measured CO content halve when switching from a case to another. High values of approximately 23,000 ppm are observed for the 150 μm – 250 μm case, while the maximum measurements go down to 12,900 ppm and 6,200 ppm for the 250 μm – 355 μm and 355 μm – 500 μm cases, respectively. For all the cases, a region with a higher content of CO is clearly identifiable along the centreline at

a certain position above the jet exit plane. The bigger the particles sizes the further downstream this peak region moves along the centreline.

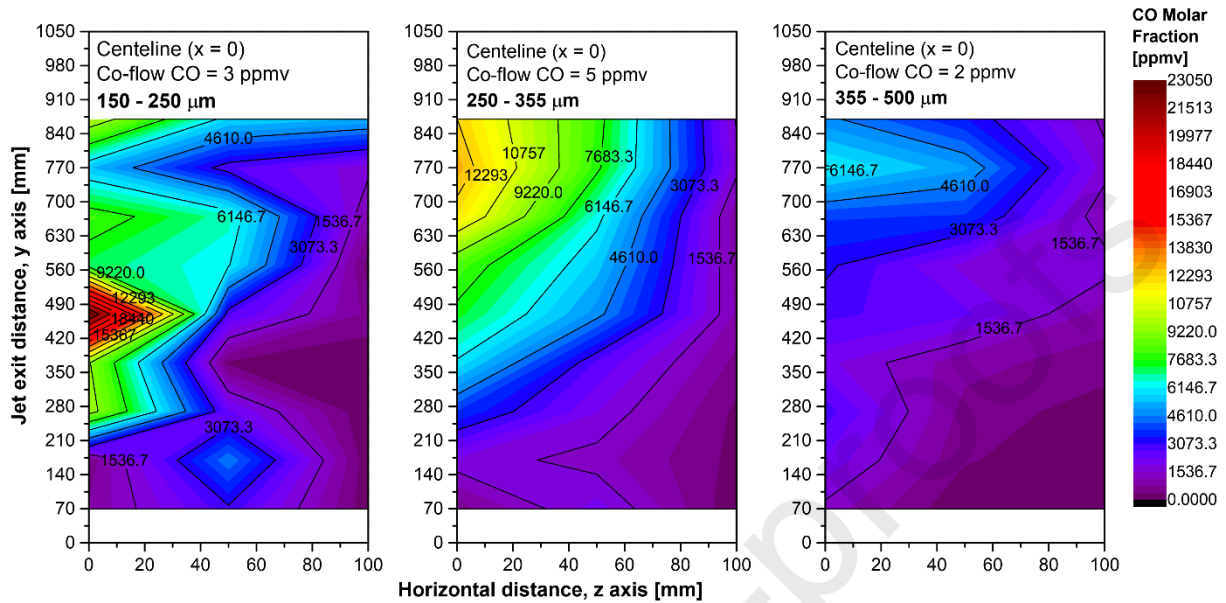


Figure 8. In-furnace CO₂ molar fraction distribution for one half in the middle of the furnace

The higher CO content for the smaller particles sizes cases can be seen as a consequence of the higher volatiles release and reaction rates. Such an observation is consistent with what has been found through the numerical analysis of the MILD combustion of brown coal [MANAB: Please add reference]. The devolatilisation process and the following volatiles combustion are directly related to the production of CO. The maximum CO molar fraction values are located along the centreline since that is the location where the volatiles release. The vertical position of this peak along the centreline depends on the time needed for the reaction to start. The shift in the location of the maximum values further downstream, with the increase of the particles' size, can be associated with a delayed devolatilisation and reaction start.

Figure 9 presents the mean O₂ molar fraction vertical profiles. The $z = 0$ mm plot shows the oxygen concentration increases initially and then plateaus for all the considered cases. This change in trend can be associated with the start of the volatile's combustion reaction.

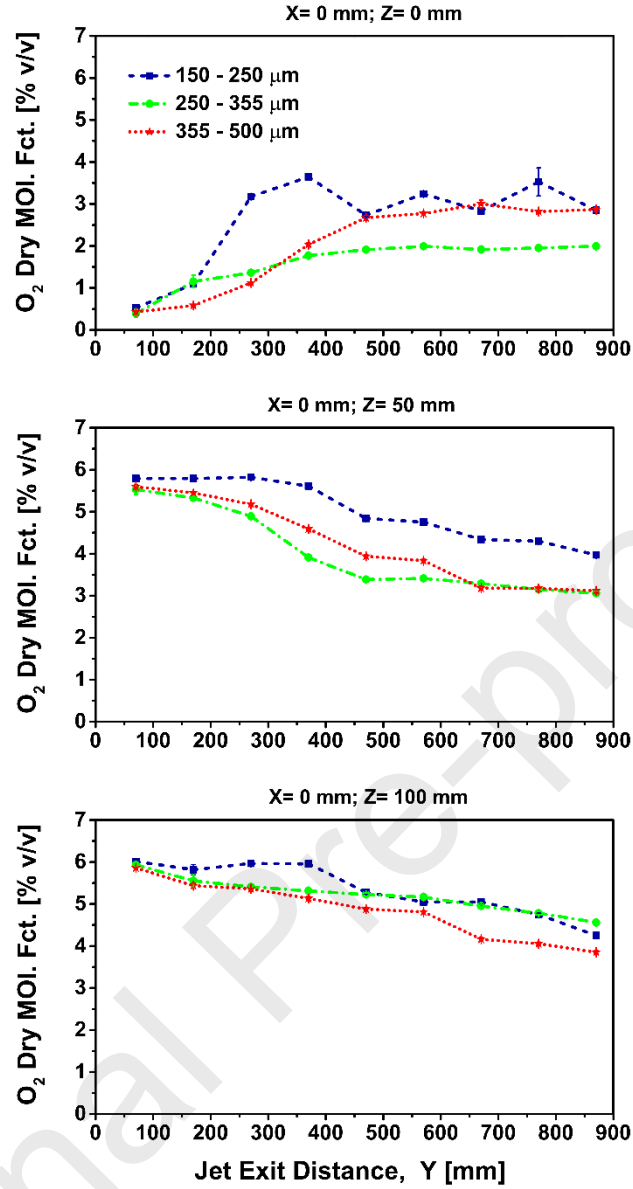


Figure 9. In-furnace O_2 molar fraction

It is possible to notice that with increasing the particles' size, the plateau extends further downstream along with the furnace. A decreasing trend of O_2 molar fraction along the y axis is observed for all the cases at the radial positions $z = 50$ mm and $z = 100$ mm. Such a reduction is more significant for the $z = 50$ mm location since it is the one closer to the shear layer where mixing and reaction with the fuel is likely to happen. Generally, the 150 μm – 250 μm case is

observed to have slightly higher values with respect to the other bigger particles sizes cases for all the radial positions investigated.

The O_2 molar fraction distribution is presented in Figure 10. A general common trend can be observed in the three studied cases. A significant O_2 gradient along the radial direction is identified at the bottom of the furnace. Here, the co-flow and central jet conditions are dominant, and this results in a low O_2 content at the centreline that rises up to values close to the 6% in the co-flow for further radial positions. For higher position, the measured mean O_2 molar fraction increases at the centreline while it becomes smaller for $z = 50$ mm and $z = 100$ mm. Such a trend leads to a smaller O_2 radial gradient for high locations along the y axis. A region characterized by low oxygen concentration with respect to the rest of the furnace is identified above the central jet exit for all particles sizes. However, this area is observed to spread further downstream and become wider in particular in the upper part with the increasing of the particles' size.

The smaller O_2 radial gradient measured at the top of the furnace is a consequence of the high recirculation and turbulence inside the furnace that allows the oxygen concentration to become more uniform. The lower O_2 overall level observed for upper locations implies that O_2 is being consumed along the length of the furnace for the volatiles and char combustion reactions. Furthermore, since the only variable between the three cases relates to the particle size, it is clear that the difference in O_2 levels relates to the devolatilisation and reaction inside the furnace. Low mean O_2 molar fraction is a consequence of a reaction and mixing with the combustion products. Hence, such a difference may indicate a different vertical location and

different spreading of the reaction zone. This seems to move further downstream and to involve a broader area with the increasing of the particles' size.

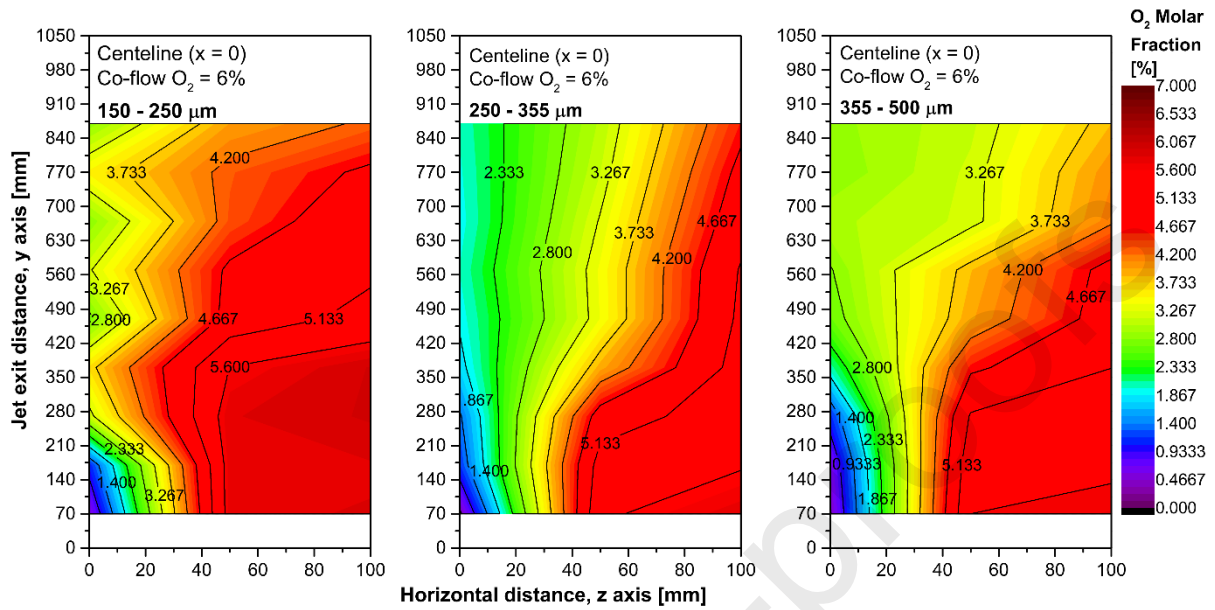


Figure 10. In-furnace O_2 molar fraction distribution for one half in the middle of the furnace

In Figure 11, the mean NO molar fraction variation along the y axis is shown. Smaller values of NO molar fraction for the $150\ \mu\text{m} - 250\ \mu\text{m}$ case, with respect to other cases, are observed for almost all radial positions, especially $z = 50\ \text{mm}$ and $z = 100\ \text{mm}$ profiles. At the $z = 0\ \text{mm}$, NO mean molar fraction profile shows a generally increasing trend among the three cases. However, similar to volatilises release, the larger particles' size the later the NO production starts. For the $150\ \mu\text{m} - 250\ \mu\text{m}$ case an early steep rise is observed, followed by a fluctuating behaviour along the upper half of the furnace. While the two other cases show a more gradual and continuous growth further downstream.

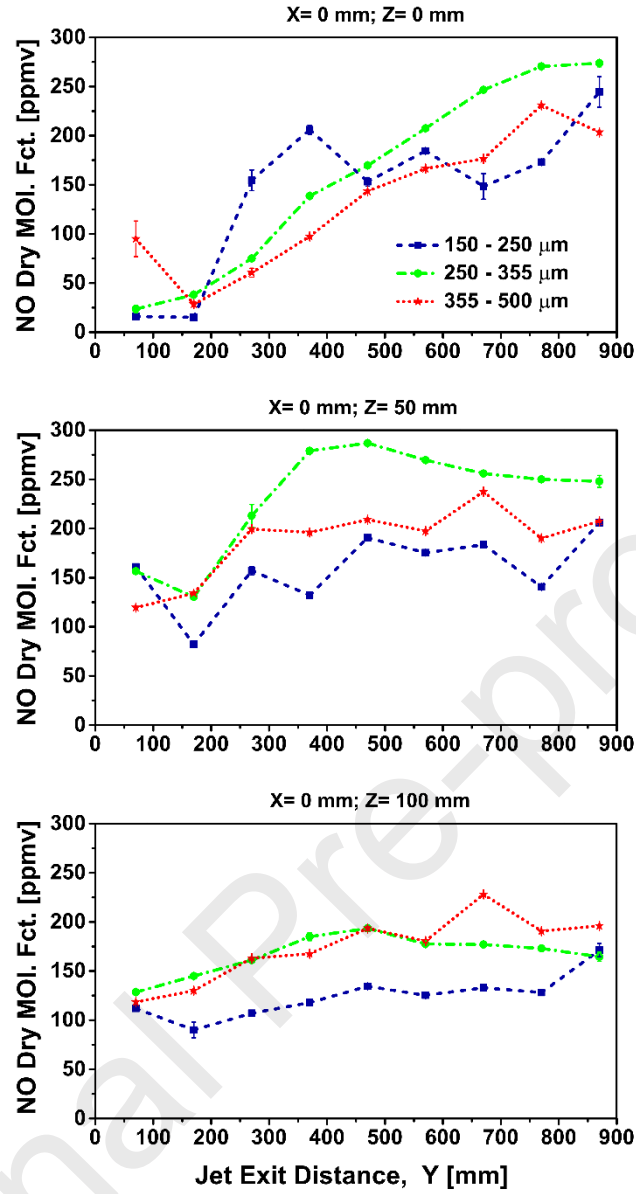


Figure 11. In-furnace NO molar fraction

The in-furnace mean NO molar fraction contours for the three particles' size cases are reported in Figure 12. The comparison shows a common trend between the three cases. Low NO values are observed at the bottom of the furnace. However, an increasing trend along the radial direction due to the different NO content between the central jet and the co-flow is highlighted. Moving upwards toward higher y-position, a sensible rise in the measured NO

molar fraction is observed for all the particle sizes along with all the radial distance. No relevant NO reduction is highlighted in an upper region of the furnace for all the cases. Generally, the overall NO content is measured to be lower for the 150 μm – 250 μm case with respect to the bigger particles sizes ones. The highest NO production is identified for the middle particles sizes cases showing a peak value of approximately 290 ppm. The 150 μm – 250 μm case distribution shows a NO production area located closer to the central jet exit and spreading less toward further radial position if compared to the other two cases. For those, NO formation zone starts further downstream along the centreline and spreads consistently along the z-axis covering a much broader area inside the furnace.

The NO production inside the furnace is dominated by the fuel-NO mechanism. The increase in NO molar fraction along the vertical direction identified for all the cases is associated with the oxidation reactions of the volatile species containing N released from the particles devolatilisation such as HCN or NH_3 . Hence, the difference observed in the high-NO content zone among the three cases can be seen as a different location along the stream and a different spreading of the volatiles reaction zone. This seems to be delayed downstream and spread more over the whole width of the furnace with the increasing of the particles sizes. The absence of a well-defined NO reduction zone in an upper region in the furnace for all the considered cases means that no NO-reburning process appears to be occurring. Further discussions are provided in the next section.

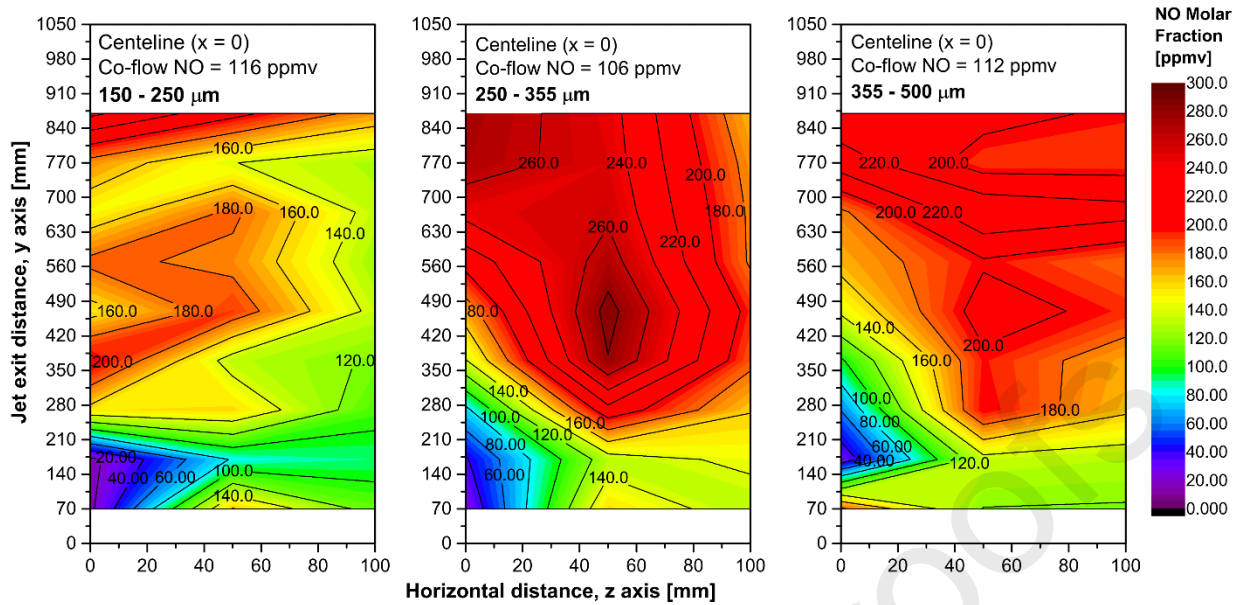


Figure 12. In-furnace NO molar fraction distribution for one half in the middle of the furnace

Exhaust Emissions

Measured mean molar fractions of O_2 , CO_2 , CO , and NO in the exhaust stream are presented in Figure 13. A single bar graph has been generated for each measured species in order to allow for comparison between the three analysed cases. Comparing the corrected NO emission levels in the exit, a little variation among the three particle sizes can be highlighted. The 250 μm – 355 μm case is observed to have the higher NO molar fraction with a value of approximately 480 ppm. The 150 μm – 250 μm case is the lowest in NO emission with a measured value of about 370 ppm, and around 400 ppm are emitted for the largest particles' case. However, it is not possible to identify a particular trend with the variation of the particles' size. Measured values in all the cases are relatively close to each other so the fuel particles' size is observed not to have a significant influence on the overall NO emissions. No remarkable NO-reburning process is observed for any cases of grape marc MILD combustion. It is interesting that NO emission was significantly, about~40% reduced via NO-reburning process

for the pulverised coal combustion [31] at the same experimental conditions of case 2. The homogeneous NO-reburning reaction largely depends on the presence of the primary species of HCN, C_xH_y , and NH_3 which are released by the devolatilisation process of solid fuels and available owing to the poor volatile combustion. Consequently, no remarkable NO-reburning for the grape marc cases point towards the intense volatile combustion.

It is worth noting that the conventional combustion of grape marc/sawdust (50/50 wt%) blend pellet in a 12-kW capacity commercial boiler produces minimum 456 mg/Nm^3 NO_x at 10% excess O_2 which is equivalent to 559 ppm at 3% excess O_2 [11]. Another study on the air-staged combustion of grape marc in a 40-kW capacity domestic size commercial boiler reveals that burning grape marc/wood pellet (50/50 wt%) blend produces 260 mg/Nm^3 at 10% excess O_2 which is equivalent to 319 ppm at 3% excess O_2 [40]. While the present study on the MILD combustion of grape marc (100 wt%) found that the minimum NO emission for the smallest particle size is measured to be 370 ppm at 3% excess O_2 . This value is similar or higher than conventional combustion mainly due to the higher N contents of 100% grape marc.

Combustion temperature plays a vital role on the NO_x emissions for the pulverised fuel combustion. It is found that below 1450°C temperature, up to 95% of the overall NO produced through fuel-NO route for the pulverised coal combustion [41]. Sun et al. [42] reported that up to 24% volatile-N and 30-50% char-N converts to NO between $1000\text{-}1300^\circ\text{C}$ temperature under the fuel-lean condition for the pulverised coal combustion. NO reduction through the NO reburning reaction is found to be higher in fuel-rich conditions than that of fuel-lean conditions [42]. This is because the majority of hydrocarbon radicals are consumed by high

concentration oxygen in an oxidising atmosphere. The maximum temperature of the present study is 1360 K ($\sim 1087^\circ\text{C}$), which is reasonably low-temperature combustion but favourable for higher fuel NO production owing to the particle residence time of at least 208 ms. The global equivalence ratio of the current experiments remains below 0.92, which is fuel lean conditions and it is speculated that the NO-reburning mechanisms appear not to be activated. A similar observation has been reported by Mendiara et al. [43], where they found that low-temperature combustion has little impact on the NO-reburning reduction under fuel-lean conditions. This issue warrants further investigation in the future perhaps through a numerical study.

CO emissions were sensibly decreasing with the increase of the particles sizes. CO molar fractions in the exhausts vary from approximately 1370 ppm in the $150\ \mu\text{m} - 250\ \mu\text{m}$ case to 660 ppm and 330 ppm in the $250\ \mu\text{m} - 355\ \mu\text{m}$ and $355\ \mu\text{m} - 500\ \mu\text{m}$ cases, respectively.

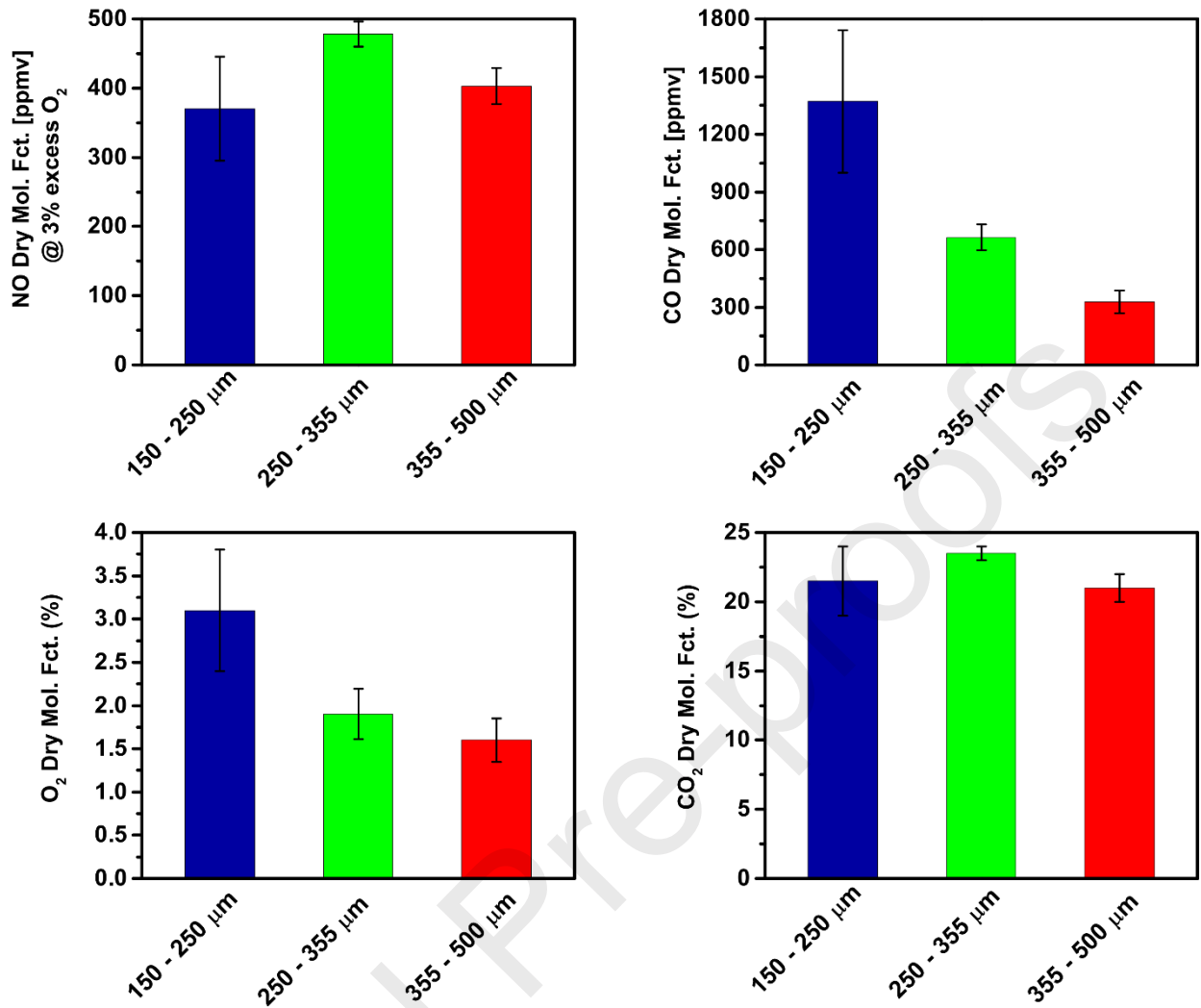


Figure 13. Exhaust gas concentrations at the exit

A well-defined O_2 decreasing trend with the increase of the particle sizes is observed in Figure 13. Such behaviour is consistent with what has been observed inside the furnace. Measured values in the exhausts range from approximately 3% for the 150 μm – 250 μm case down to 2% and 1.5% for the 250 μm – 355 μm and 355 μm – 500 μm cases, respectively.

These values are slightly smaller than the one's observed at higher vertical locations inside the furnace. Such behaviour means that combustion reactions continue inside the furnace on the way to the exhaust's outlet duct. However, the reduction of oxygen content in the exhaust gases for larger particles cases is in contradiction with what was found for the brown coal

MILD combustion [31]. Figure 13 also presents the CO₂ content comparison. Only a little variation is observed among the considered cases which values stay in a range between 20% and 23%. No defined trend has been identified for the CO₂ molar fraction in the exhausts with the increase of the particles' sizes.

Worth noting is that the present study focuses on the MILD combustion characteristics of grape marc for a fixed residence time of particles as well as a constant jet Reynolds number. A strong recirculation zone is established halfway along the furnace with the estimated particles residence time of 246 ms and 136 ms, when burning pulverised coal MILD combustion under the same operating conditions [25, 31]. Also, a reasonably strong NO reduction through reburn mechanism was found for the MILD combustion of pulverised brown coal [31], while no reburning effect is encountered for the grape marc combustion. Although the N contents between brown coal and grape marc are significantly different [6], a detail modelling study is necessary to better understand the kinetics under these conditions.

Conclusions

This paper reports the results from an experimental investigation which is focused on the burning characteristics of grape marc particles inside a vertical furnace operating under MILD combustion conditions. In particular, the study examines the effect of grape marc particles size on the flame structure, stability and pollutant emissions under MILD combustion. Three ranges of particle sizes are investigated while all other experimental conditions remained exactly the same. No visible flame has been observed for any of the experimental cases and a semi-uniform thermal field was measured inside the furnace. This demonstrates that MILD combustion conditions have been successfully achieved for all cases. The case of the largest

particle size exhibits a higher mean temperature by ~40K as compared to the other two cases. The resulting high temperature is believed to be related to the intense volatile oxidation of the largest particles' case (355 – 500 μm) and consequently, a significant reduction of the exhaust CO is observed compared with the other two cases. The highest NO production is identified for the middle particles' size case (250 μm – 355 μm) showing a peak value of approximately 478 ppm in the exhaust, while the lowest NO emission was recorded for the lowest particle size case (150 – 255 μm) at 370 ppm, all corrected for 3% excess O_2 . No remarkable NO-reburning process is observed for any cases owing to the absence of a NO reduction zone in an upper region of the furnace. Future work should explore the underpinning reasons for the apparent lack of a NO-reburning mechanism through a detailed modelling study.

Acknowledgments

The authors appreciate Mr Marc Simpson, Manager, Thebarton Research Laboratory, The University of Adelaide for his help throughout the experiments.

Declarations of Interest: None

References

- [1] M.F. Demirbas, M. Balat, H. Balat, Potential contribution of biomass to the sustainable energy development, *Energy Convers. Manage.* 50 (2009) 1746-1760.
<https://doi.org/10.1016/j.enconman.2009.03.013>
- [2] A. Demirbaş, Global renewable energy resources, *Energy Sources Part A.* 28 (2006) 779-792.
<https://doi.org/10.1080/00908310600718742>

- [3] M. Balat, Energy and greenhouse gas emissions: a global perspective, *Energy Sources Part B*. 1 (2006) 157-170. <https://doi.org/10.1080/009083190881571>
- [4] M. Hoogwijk, A. Faaij, B. Eickhout, B. de Vries, W. Turkenburg, Potential of biomass energy out to 2100, for four IPCC SRES land-use scenarios, *Biomass Bioenergy*. 29 (2005) 225-257. <https://doi.org/10.1016/j.biombioe.2005.05.002>
- [5] REN21 Secretariat, Renewables 2019 Global Status Report, in, Paris, France, <https://www.ren21.net/reports/global-status-report/>, 2019 (accessed 20 Dec 2019).
- [6] M. Saha, G. Gitto, A. Chinnici, B.B. Dally, Comparative study of the MILD combustion characteristics of biomass and brown coal, *Energy Fuels*. 32 (2018) 4202-4211. <https://doi.org/10.1021/acs.energyfuels.7b03158>
- [7] Wine Australia, Recovery of valuable products from lees and integrated approach to minimise waste and add value to wine production, <https://www.wineaustralia.com/research/projects/recovery-of-valuable-products-from-lees/>, 2003 (accessed 20 Dec 2019).
- [8] Winemakers Federation of Australia, National Vintage Report 2017, https://www.wineaustralia.com/getmedia/12acee4d-d39f-475c-9fac-bff5674f2f28/NationalVintageReport_2017_withappendix/, 2017 (accessed 20 Dec 2019).
- [9] R.A. Muhlack, R. Potumarthi, D.W. Jeffery, Sustainable wineries through waste valorisation: A review of grape marc utilisation for value-added products, *Waste Manage*. 72 (2018) 99-118. <https://doi.org/10.1016/j.wasman.2017.11.011>
- [10] M.T. Miranda, J.I. Arranz, S. Román, S. Rojas, I. Montero, M. López, J.A. Cruz, Characterization of grape pomace and pyrenean oak pellets, *Fuel Process. Technol*. 92 (2011) 278-283. <https://doi.org/10.1016/j.fuproc.2010.05.035>
- [11] N. Kraiem, M. Lajili, L. Limousy, R. Said, M. Jeguirim, Energy recovery from Tunisian agri-food wastes: Evaluation of combustion performance and emissions characteristics of green pellets prepared from tomato residues and grape marc, *Energy*. 107 (2016) 409-418. <https://doi.org/10.1016/j.energy.2016.04.037>
- [12] EPA, United States Environmental Protection Agency, Particulate Matter (PM) Pollution (2017), <http://www.epa.gov/pm-pollution/>, (accessed 24 Dec 2019).
- [13] X. Zhang, Emission standards and control of PM_{2.5} from coal-fired power plant, in: IEA Clean Coal Centre, IEA Clean Coal Centre, London, UK, 2016, pp. 26-38.
- [14] S. Adhikari, N. Abdoulmoumine, H. Nam, O. Oyediji, Biomass gasification producer gas cleanup, in: *Bioenergy Systems for the Future*, Elsevier, 2017, pp. 541-557.
- [15] C. Schönnenbeck, G. Trouvé, M. Valente, P. Garra, J. Brilhac, Combustion tests of grape marc in a multi-fuel domestic boiler, *Fuel*, 180 (2016) 324-331. <https://doi.org/10.1016/j.fuel.2016.04.034>
- [16] D. Yu, C. Wen, M. Xu, Effect of Low-NO_x Combustion on PM₁₀ Emissions from Pulverized-Coal-Fired Boilers, *Energy Fuels*, 27 (2013) 5811-5815. <https://doi.org/10.1021/ef401182k>

- [17] M. McElroy, R. Carr, D. Ensor, G. Markowski, Size distribution of fine particles from coal combustion, *Science*, 215 (1982) 13-19. <https://doi.org/10.1126/science.215.4528.13>
- [18] E. Mastorakos, A.M.K.P. Taylor, J.H. Whitelaw, Extinction of turbulent counterflow flames with reactants diluted by hot products, *Combust. Flame*, 102 (1995) 101-114. [https://doi.org/10.1016/0010-2180\(94\)00252-N](https://doi.org/10.1016/0010-2180(94)00252-N)
- [19] A. Cavaliere, M. de Joannon, Mild combustion, *Prog. Energy Combust. Sci.* 30 (2004) 329-366. <https://doi.org/10.1016/j.pecs.2004.02.003>
- [20] R. Weber, J.P. Smart, W. Kamp, On the (MILD) combustion of gaseous, liquid, and solid fuels in high temperature preheated air, *Proc. Combust. Inst.*, 30 (2005) 2623-2629. <https://doi.org/10.1016/j.proci.2004.08.101>
- [21] J. Smart, G. Riley, Combustion of coal in a flameless oxidation environment under oxyfuel firing conditions: the reality, *J. Energy Inst.* 85 (2012) 131-134.
- [22] M. Saha, B.B. Dally, P.R. Medwell, E.M. Cleary, Moderate or Intense Low Oxygen Dilution (MILD) combustion characteristics of pulverized coal in a self-recuperative furnace, *Energy Fuels*. 28 (2014) 6046-6057. <https://doi.org/10.1021/ef5006836>
- [23] P. Li, F. Wang, Y. Tu, Z. Mei, J. Zhang, Y. Zheng, H. Liu, Z. Liu, J. Mi, C. Zheng, Moderate or Intense Low-Oxygen Dilution Oxy-combustion characteristics of light oil and pulverized coal in a pilot-scale furnace, *Energy Fuels*, 28 (2014) 1524-1535. <https://doi.org/10.1021/ef402240w>
- [24] M. Weidmann, D. Honoré, V. Verbaere, G. Boutin, S. Grathwohl, G. Godard, C. Gobin, R. Kneer, G. Scheffknecht, Experimental characterization of pulverized coal MILD flameless combustion from detailed measurements in a pilot-scale facility, *Combust. Flame*. 168 (2016) 365-377. <https://doi.org/10.1016/j.combustflame.2016.01.029>
- [25] M. Saha, B.B. Dally, P.R. Medwell, A. Chinnici, Burning characteristics of Victorian brown coal under MILD combustion conditions, *Combust. Flame*. 172 (2016) 252-270. <https://doi.org/10.1016/j.combustflame.2016.07.026>
- [26] Z. Mei, P. Li, J. Mi, F. Wang, J. Zhang, Diffusion MILD combustion of firing pulverized-coal at a pilot furnace, *Flow Turbul. Combust.* 95 (2015) 803-829. <https://doi.org/10.1007/s10494-015-9642-0>
- [27] M. Saha, A. Chinnici, B.B. Dally, P.R. Medwell, Numerical study of pulverized coal MILD combustion in a self-recuperative furnace, *Energy Fuels*. 29 (2015) 7650-7669. <https://doi.org/10.1021/acs.energyfuels.5b01644>
- [28] M. Saha, B.B. Dally, A. Chinnici, P.R. Medwell, Effect of co-flow oxygen concentration on the MILD combustion of pulverised coal, *Fuel Process. Technol.* 193 (2019) 7-18. <https://doi.org/10.1016/j.fuproc.2019.04.033>
- [29] S.-J. Zhu, Q.-G. Lyu, J.-G. Zhu, J.-R. Li, NO emissions under pulverized char MILD combustion in O₂/CO₂ preheated by a circulating fluidized bed: Effect of oxygen-staging gas distribution, *Fuel Process. Technol.* 182 (2018) 104-112. <https://doi.org/10.1016/j.fuproc.2018.09.002>
- [30] Z. Zhang, X. Li, L. Zhang, C. Luo, B. Lu, Y. Xu, J. Liu, A. Chen, C. Zheng, Effect of H₂O/CO₂ mixture on heat transfer characteristics of pulverized coal MILD-oxy combustion, *Fuel Process. Technol.* 184 (2019) 27-35. <https://doi.org/10.1016/j.fuproc.2018.11.011>

- [31] M. Saha, B.B. Dally, P.R. Medwell, A. Chinnici, Effect of particle size on the MILD combustion characteristics of pulverised brown coal, *Fuel Process. Technol.* 155 (2017) 74-87. <https://doi.org/10.1016/j.fuproc.2016.04.003>
- [32] Z. Mei, P. Li, F. Wang, J. Zhang, J. Mi, Influences of reactant injection velocities on moderate or intense low-oxygen dilution coal combustion, *Energy Fuels*. 28 (2013) 369-384. <https://doi.org/10.1021/ef401509e>
- [33] B. Luo, X.-Q. Ma, NO_x formed specialty of biomass fuel in HTAC, ASME Power Conference, 2008, pp. 1427-1431. <https://doi.org/10.1115/PWR2005-50333>
- [34] P. Anna, W. Yang, W. Blasiak, Combustion of solid fuels under the conditions of high temperature and various oxygen concentration, in: *Challenges of Power Engineering and Environment*, Springer Publications, Germany, 2007, pp. 871-876.
- [35] G.-M. Choi, M. Katsuki, Advanced low NO_x combustion using highly preheated air, *Energy Convers. Manage.* 42 (2001) 639-652. [https://doi.org/10.1016/S0196-8904\(00\)00074-1](https://doi.org/10.1016/S0196-8904(00)00074-1)
- [36] R. Weber, Y. Poyraz, A.M. Beckmann, S. Brinker, Combustion of biomass in jet flames, *Proc. Combust. Inst.*, 35 (2015) 2749-2758. <https://doi.org/10.1016/j.proci.2014.06.033>
- [37] J. Li, W. Yang, W. Blasiak, A. Ponzio, Volumetric combustion of biomass for CO₂ and NO_x reduction in coal-fired boilers, *Fuel*. 102 (2012) 624-633. <https://doi.org/10.1016/j.fuel.2012.06.083>
- [38] X. Wang, J. Zhang, X. Xu, H. Mikulčić, Y. Li, Y. Zhou, H. Tan, Numerical study of biomass Co-firing under Oxy-MILD mode, *Renewable Energy*. 146 (2020) 2566-2576. <https://doi.org/10.1016/j.renene.2019.08.108>
- [39] B. Alganash, M.C. Paul, I.A. Watson, Numerical investigation of the heterogeneous combustion processes of solid fuels, *Fuel*. 141 (2015) 236-249. <https://doi.org/10.1016/j.fuel.2014.10.060>
- [40] C. Schönnenbeck, G. Trouvé, M. Valente, P. Garra, J.F. Brilhac, Combustion tests of grape marc in a multi-fuel domestic boiler, *Fuel*. 180 (2016) 324-331. <https://doi.org/10.1016/j.fuel.2016.04.034>
- [41] B.G. Miller, *Clean coal engineering technology*, Elsevier, Kidlington, Oxford, UK, 2010, PP. 110-115. <https://doi.org/10.1016/B978-1-85617-710-8.00004-2>
- [42] S. Sun, H. Cao, H. Chen, X. Wang, J. Qian, T. Wall, Experimental study of influence of temperature on fuel-N conversion and recycle NO reduction in oxyfuel combustion, *Proc. Combust. Inst.*, 33 (2011) 1731-1738. <https://doi.org/10.1016/j.proci.2010.06.014>
- [43] T. Mendiara, P. Glarborg, Reburn chemistry in oxy-fuel combustion of methane, *Energy Fuels*, 23 (2009) 3565-3572. <https://doi.org/10.1021/ef9001956>

BURNING CHARACTERISTICS OF GRAPE MARC UNDER MILD COMBUSTION CONDITIONS

Manabendra Saha^{*}, Giovanni Gitto and Bassam B. Dally

Centre for Energy Technology, School of Mechanical Engineering,

The University of Adelaide, SA 5005, Australia

Author Statement

Manabendra Saha: Conceptualization, Methodology, Data Analysis, Writing- Original draft preparation, Reviewing and Editing.

BURNING CHARACTERISTICS OF GRAPE MARC UNDER MILD COMBUSTION CONDITIONS

Manabendra Saha^{*}, Giovanni Gitto and Bassam B. Dally

Centre for Energy Technology, School of Mechanical Engineering,

The University of Adelaide, SA 5005, Australia

Declaration of interests

☒ The authors declare that they have no known competing financial interests or personal relationships that could have appeared to influence the work reported in this paper.

☐ The authors declare the following financial interests/personal relationships which may be considered as potential competing interests:

--

BURNING CHARACTERISTICS OF GRAPE MARC UNDER MILD COMBUSTION CONDITIONS

HIGHLIGHTS:

- MILD combustion characteristics of grape marc are experimentally investigated
 - No visible flame has observed for any of the experimental cases
 - A semi-uniform thermal field was measured inside the furnace
 - The highest NO is produced for the 250 μm – 355 μm sized particles' case
 - No remarkable NO-reburning process is found for any cases
-